Numer. Math. (2010) 115:647–679
DOI 10.1007/s00211-010-0289-4

Numerische Mathematik

A multiwave approximate Riemann solver for ideal MHD based on relaxation II: numerical implementation with 3 and 5 waves

François Bouchut · Christian Klingenberg · Knut Waagan

Received: 20 May 2008 / Revised: 23 November 2009 / Published online: 2 March 2010

Abstract In the first part of this work Bouchut et al. (J Comput Phys 108:7–41, 2007) we introduced an approximate Riemann solver for one-dimensional ideal MHD derived from a relaxation system. We gave sufficient conditions for the solver to satisfy discrete entropy inequalities, and to preserve positivity of density and internal energy. In this paper we consider the practical implementation, and derive explicit wave speed estimates satisfying the stability conditions of Bouchut et al. (J Comput Phys 108:7–41, 2007). We present a 3-wave solver that well resolves fast waves and material contacts, and a 5-wave solver that accurately resolves the cases when two eigenvalues coincide. A full 7-wave solver, which is highly accurate on all types of waves, will be described in a follow-up paper. We test the solvers on one-dimensional shock tube data and smooth shear waves.

Mathematics Subject Classification (2000) 76M12 · 65M12 · 76W05

F. Bouchut
Département de Mathématiques et Applications, CNRS & Ecole Normale Supérieure,
45 rue d'Ulm, 75230 Paris cedex 05, France
e-mail: Francois.Bouchut@ens.fr

F. Bouchut (✉)
CNRS & LAMA Université Paris-Est Marne-la-Vallée, 5 Boulevard Descartes Cité Descartes,
Champs-sur-Marne, 77454 Marne-la-Vallée cedex 2, France
e-mail: francois.bouchut@univ-mlv.fr

C. Klingenberg
Department of Mathematics, Würzburg University, Am Hubland, 97074 Würzburg, Germany
e-mail: klingenberg@mathematik.uni-wuerzburg.de

K. Waagan
High Altitude Observatory, National Center for Atmospheric Research,
P.O. Box 3000, Boulder, CO 80307-3000, USA
e-mail: knut.waagan@cma.uio.no

1 Introduction

The equations for ideal MHD in one dimension are

$$\rho_t + (\rho u)_x = 0, \tag{1.1}$$

$$(\rho u)_t + \left(\rho u^2 + p + \frac{1}{2}|B_\perp|^2 - \frac{1}{2}B_x^2\right)_x = 0, \tag{1.2}$$

$$(\rho u_\perp)_t + (\rho u u_\perp - B_x B_\perp)_x = 0, \tag{1.3}$$

$$E_t + \left[\left(E + p + \frac{1}{2}|B_\perp|^2 - \frac{1}{2}B_x^2\right)u - B_x(B_\perp \cdot u_\perp)\right]_x = 0, \tag{1.4}$$

$$(B_\perp)_t + (B_\perp u - B_x u_\perp)_x = 0. \tag{1.5}$$

The state variables are the mass density ρ, the pressure p, the velocity split into its longitudinal and transverse components u and $u_\perp$, and the magnetic field similarly into B_x and $B_\perp$. Hence $u_\perp$ and $B_\perp$ are two-dimensional vectors. Since the divergence of the magnetic field is zero at all times, we take B_x constant for one-dimensional data, but that restriction may be relaxed. Finally there is the total energy E,

$$E = \frac{1}{2}\rho(u^2 + |u_\perp|^2) + \rho e + \frac{1}{2}(B_x^2 + |B_\perp|^2), \tag{1.6}$$

with e denoting the specific internal energy. The system is closed by an equation of state $p = p(\rho, e)$. Thermodynamical considerations leads to the assumption of existence of a specific physical entropy $s = s(\rho, e)$ that satisfies

$$de + p\, d\left(\frac{1}{\rho}\right) = T ds \tag{1.7}$$

for some temperature $T(\rho, e) > 0$. To ensure the hyperbolicity of (1.1)–(1.5), we assume that

$$p' \equiv \left(\frac{\partial p}{\partial \rho}\right)_s > 0, \tag{1.8}$$

where the subscript s means that the partial derivative is taken with s constant. We shall also make the classical assumption that

$$-s \text{ is a convex function of } \left(\frac{1}{\rho}, e\right). \tag{1.9}$$

This is a follow-up paper to [5] where we proposed an approximate Riemann solver for (1.1)–(1.5). It is based on a relaxation approximation which generalized the Suliciu relaxation approach for the Euler equations, see [2,3]. In Sect. 1.1 of [5] we described Godunov schemes and the idea of approximate Riemann solvers. We then introduced discrete entropy inequalities as a stability constraint, which can be seen also as a way to numerically impose the second law of thermodynamics. A second important

stability criterion is the positivity of density and internal energy. In Sect. 1.2 we discussed positivity and entropy inequalities in the context of relaxation systems. This was exemplified by the Suliciu relaxation system for the Euler equations, that our relaxation system for (1.1)–(1.5) generalizes.

In the next section we recall the results of [5]. In Sect. 3 we describe our approximate Riemann solvers with 3 and 5 waves that are special cases of our underlying approach. We give explicit formulas for wave speeds that ensure entropy inequalities and positivity in both the 3-wave and the 5-wave case. These formulas are extensions of the explicit signal speeds for the HLLC solver introduced in [3]. Finally we run some numerical tests. Our solvers are compared against each other and against the Roe solver, the HLL solver, and the 5-wave solver of [11]. At the end we summarize the results. In a follow-up paper [4] we treat the case of the full 7-wave solver.

In multidimensional simulations, one-dimensional solvers are commonly used as building blocks. In the case of ideal MHD the constraint that $\operatorname{div} B = 0$ is an additional challenge. We describe in an appendix how Powell's idea of extending (1.1)–(1.5), see [12], can be easily incorporated into our relaxation approach. Other methods used in the multidimensional finite volume setting should in principle be able to use our one-dimensional solver.

2 Relaxation system and approximate Riemann solver

In [5] we introduced the relaxation system

$$\rho_t + (\rho u)_x = 0, \tag{2.1}$$

$$(\rho u)_t + (\rho u^2 + \pi)_x = 0, \tag{2.2}$$

$$(\rho u_\perp)_t + (\rho u u_\perp + \pi_\perp)_x = 0, \tag{2.3}$$

$$E_t + [(E + \pi)u + \pi_\perp \cdot u_\perp]_x = 0, \tag{2.4}$$

$$(B_\perp)_t + (B_\perp u - B_x u_\perp)_x = 0, \tag{2.5}$$

with still (1.6), and where the relaxation pressures π and $\pi_\perp$ evolve according to

$$(\rho\pi)_t + (\rho\pi u)_x + (|b|^2 + c_b^2)u_x - c_a b \cdot (u_\perp)_x = 0, \tag{2.6}$$

$$(\rho\pi_\perp)_t + (\rho\pi_\perp u)_x - c_a b\, u_x + c_a^2 (u_\perp)_x = 0. \tag{2.7}$$

The parameters $c_a \geq 0, c_b \geq 0$, and $b \in \mathbf{R}^2$ play the role of approximations of $\sqrt{\rho}|B_x|$, $\rho\sqrt{p'}$ and $\operatorname{sign}(B_x)\sqrt{\rho}B_\perp$ respectively. Indeed, c_a, c_b, b are not taken constant, but are evolved with

$$(c_a)_t + u(c_a)_x = 0, \quad (c_b)_t + u(c_b)_x = 0, \quad b_t + u b_x = 0. \tag{2.8}$$

The eigenvalues of the system (2.1)–(2.8) are $u, u \mp \frac{c_s}{\rho}, u \mp \frac{c_a}{\rho}$ and $u \mp \frac{c_f}{\rho}$, where

$$\begin{aligned} c_s^2 &= \frac{1}{2}\left(c_b^2 + c_a^2 + |b|^2 - \sqrt{(c_b^2 + c_a^2 + |b|^2)^2 - 4c_a^2 c_b^2}\right), \\ c_f^2 &= \frac{1}{2}\left(c_b^2 + c_a^2 + |b|^2 + \sqrt{(c_b^2 + c_a^2 + |b|^2)^2 - 4c_a^2 c_b^2}\right), \end{aligned} \tag{2.9}$$

u having multiplicity 8. All are linearly degenerate. Note that $c_s \le c_a \le c_f, c_s \le c_b \le c_f$, and that the eigenvalues of (2.1)–(2.8) equal the eigenvalues of (1.1)–(1.5) whenever $c_a = \sqrt{\rho}|B_x|$, $c_b = \rho\sqrt{p'}$ and $b = \mathrm{sign}(B_x)\sqrt{\rho}B_\perp$. However, in order to simplify, we shall make here different choices, leading to a solver with 3 waves or 5 waves instead of 7 waves. The full motivation for the relaxation system is given in Sect. 2 of [5].

The approximate Riemann solver associated to the above relaxation system is a function $R(x/t, U_l, U_r)$, where U stands for the MHD variable $U = (\rho, \rho u, \rho u_\perp, E, B_\perp)$. It is obtained by solving the Riemann problem for (2.1)–(2.8), and dropping the extra components $\pi, \pi_\perp, c_a, c_b, b$. Initially, this Riemann problem starts with the relaxation pressures at equilibrium,

$$\pi = p + \frac{1}{2}|B_\perp|^2 - \frac{1}{2}B_x^2 \quad \text{and} \quad \pi_\perp = -B_x B_\perp. \tag{2.10}$$

The signal speeds c_a, c_b, b have to be specified initially on the left and on the right, i.e. one has to give values for

$$c_{bl},\ c_{br},\ c_{al},\ c_{ar},\ b_l,\ b_r. \tag{2.11}$$

This choice is the key issue for stability and accuracy. This approximate Riemann solver is consistent with (1.1)–(1.5) and conservative, whatever is the choice of these signal speeds (see [3] for the precise meaning of this). Our relaxation system (2.1)–(2.8) generalizes the Suliciu relaxation system for gas dynamics, hence since the HLLC solver is associated to the Suliciu system, our approximate Riemann solver is an extension of the HLLC solver to MHD.

If the initial data U_l, U_r consist of a single material contact discontinuity, the approximate Riemann solver gives the exact solution to (1.1)–(1.5), π and $\pi_\perp$ remaining at equilibrium. Isolated Alfven contact discontinuities are as well exactly resolved under some additional conditions specified in [5]. These additional conditions cannot be satisfied for the 3-wave or 5-wave solvers considered here.

As usual, an approximate Riemann solver leads to a conservative scheme

$$U_i^{n+1} = U_i^n - \frac{\Delta t}{\Delta x}\left(F^n_{i+\frac{1}{2}} - F^n_{i-\frac{1}{2}}\right), \tag{2.12}$$

where the index i refers to the cell, the index n to time, and

$$F^n_{i+1/2} = \mathcal{F}(U_i^n, U_{i+1}^n) \tag{2.13}$$

with $\mathcal{F}(U_l, U_r)$ the numerical flux. In our case, since our solver $R(x/t, U_l, U_r)$ comes from the exact solution to (2.1)–(2.8) which is conservative in U, it is given by the exact flux of (2.1)–(2.8) evaluated at $x/t = 0$,

$$\mathcal{F}(U_l, U_r) = (\rho u, \rho u^2 + \pi, \rho u u_\perp + \pi_\perp, (E + \pi)u + \pi_\perp \cdot u_\perp, B_\perp u - B_x u_\perp)_{x/t=0}. \tag{2.14}$$

The CFL-condition for this scheme is

$$\max\left(\left|u_l - \frac{c_{fl}}{\rho_l}\right|, \left|u_r + \frac{c_{fr}}{\rho_r}\right|\right)\Delta t \leq C\Delta x, \tag{2.15}$$

for some CFL-number C. A value $C = 1/2$ ensures that the waves emerging from the cell interfaces do not interact. However, it is common in practice to use $C = 1$ for the first-order scheme.

Since all characteristic fields of (2.1)–(2.8) are linearly degenerate, the Riemann problem is much easier to solve than for the original MHD system. Indeed its solution consists of constant states (we shall call them "intermediate states" in the sequel), separated by discontinuities. In order to get the solution one has only to list the weak Riemann invariants associated to each eigenvalue, and to write that each of them does not jump through the associated discontinuity.

The aim of this work is to produce an accurate, positive and entropy satisfying approximate Riemann solver for MHD. By entropy satisfying we mean that the scheme (2.12) satisfies discrete entropy inequalities

$$\eta(U_i^{n+1}) \leq \eta(U_i^n) - \frac{\Delta t}{\Delta x}\left(G^n_{i+\frac{1}{2}} - G^n_{i-\frac{1}{2}}\right) \tag{2.16}$$

for entropy flux pairs (η, G), where $G^n_{i+\frac{1}{2}} = \mathcal{G}(U_i^n, U_{i+1}^n)$, and $\mathcal{G}(U_l, U_r)$ is a numerical entropy flux, satisfying $\mathcal{G}(U, U) = G(U)$. For ideal MHD we consider $\eta = \rho\phi(s)$, and $G = \eta u$, where ϕ is any decreasing and convex function. The assumption (1.9) ensures that $\eta = \rho\phi(s)$ is convex with respect to U. A stronger entropy inequality can indeed be formulated on the approximate Riemann solver itself (see [3]). The positivity of density and internal energy for the approximate Riemann solver (i.e. for its intermediate values) is also retained as the useful formulation, instead of the weaker one stating that the scheme (2.12) is positive.

In [5] we derived stability conditions, that ensure that the approximate Riemann solver is positive and entropy satisfying. These stability conditions must hold for each intermediate state of the approximate solver, and involve also the initial states and the relaxation parameters (2.11). It is convenient to denote by a star any value corresponding to an intermediate state, while the sub- or superscript 'l/r' will be used to refer to the initial state on the same side of the central wave as the intermediate value considered. In [5] we proved the following result.

Proposition 2.1 *The approximate Riemann solver defined by the relaxation system* (2.1)–(2.8) *is positive and satisfies the discrete entropy inequalities if, for each*

intermediate state, denoted by a star, we have $\rho^* > 0$ *and*

$$\begin{aligned} &(\rho^2 p')_{*,l/r} \le c_b^2, \qquad \frac{1}{\rho^*} - \frac{B_x^2}{c_a^2} \ge 0, \\ &\left| B_\perp^{l/r} - B_x \frac{b}{c_a} \right|^2 \le \left(c_b^2 - (\rho^2 p')_{*,l/r} \right) \left(\frac{1}{\rho^*} - \frac{B_x^2}{c_a^2} \right), \end{aligned} \tag{2.17}$$

where $(\rho^2 p')_{*,l/r}$ *is defined as*

$$(\rho^2 p')_{*,l/r} \equiv \sup_{\rho \in [\rho_{l/r}, \rho^*]} \rho^2 p'(\rho, s_{l/r}), \tag{2.18}$$

and where c_b, c_a, b *are evaluated locally, i.e. they stand for* $c_{b,l/r}, c_{a,l/r}, b_{l/r}$.

3 Riemann solvers with 3 and 5 waves

The solvers considered in this paper are obtained with the choice $b_l = b_r = 0$. This makes the formulas for the intermediate states simpler, resulting in fast codes and a relatively simple analysis.

3.1 Intermediate states for the 3-wave solver

The most simple choice for the signal speeds is obtained by taking

$$b = 0, \qquad c_a = c_b \equiv c, \tag{3.1}$$

which means that we have only two parameters $c_l > 0$, $c_r > 0$. Then $c_s = c_f = c$, thus we have only three eigenvalues for the system (2.1)–(2.8), which are $u - c/\rho$, u, $u + c/\rho$. This leads to a solver with 3 waves and 2 intermediate states, that will be denoted as l^* and r^*.

The left and right waves have multiplicity 3. There are 8 strong Riemann invariants associated to the central wave (i.e. quantities that lie in the kernel of $\partial_t + u\partial_x$), which are c_a, c_b, b, and

$$\frac{1}{\rho} + \frac{\pi}{c^2}, \qquad \frac{B_\perp}{\rho} + \frac{B_x}{c^2}\pi_\perp, \qquad e + \frac{B_x^2 + |B_\perp|^2}{2\rho} - \frac{\pi^2}{2c^2} - \frac{|\pi_\perp|^2}{2c^2}. \tag{3.2}$$

These quantities are thus weak Riemann invariants for the left and right waves. They must be completed with 3 weak Riemann invariants, that are found to be $\pi + cu$, $\pi_\perp + cu_\perp$ for the left wave, and $\pi - cu$, $\pi_\perp - cu_\perp$ for the right wave. For the central wave, 6 weak Riemann invariants are u, $u_\perp$, π, $\pi_\perp$. The wave speeds are therefore $\sigma_1 < \sigma_2 < \sigma_3$,

$$\sigma_1 = u_l - \frac{c_l}{\rho_l}, \quad \sigma_2 = u_l^* = u_r^* \equiv u^*, \quad \sigma_3 = u_r + \frac{c_r}{\rho_r}. \tag{3.3}$$

The values of c_a, c_b, b are the left values for the l^* state, and the right values for the r^* state. The intermediate values for $\rho, B_\perp, e$ are deduced from the fact that the quantities in (3.2) do not jump through the left and right waves. It remains to determine the values $u^*, u^*_\perp, \pi^*, \pi^*_\perp$ (which are common for the l^* and r^* states). They are determined by the relations

$$\begin{aligned} (\pi + cu)^*_l &= (\pi + cu)_l, \qquad (\pi - cu)^*_r = (\pi - cu)_r, \\ (\pi_\perp + cu_\perp)^*_l &= (\pi_\perp + cu_\perp)_l, \qquad (\pi_\perp - cu_\perp)^*_r = (\pi_\perp - cu_\perp)_r. \end{aligned} \tag{3.4}$$

Hence we get the intermediate values

$$\begin{aligned} u^* &= \frac{c_l u_l + c_r u_r + \pi_l - \pi_r}{c_l + c_r}, \\ \pi^* &= \frac{c_r \pi_l + c_l \pi_r - c_l c_r (u_r - u_l)}{c_l + c_r}, \\ u^*_\perp &= \frac{c_l u^l_\perp + c_r u^r_\perp + \pi^l_\perp - \pi^r_\perp}{c_l + c_r}, \\ \pi^*_\perp &= \frac{c_r \pi^l_\perp + c_l \pi^r_\perp - c_l c_r (u^r_\perp - u^l_\perp)}{c_l + c_r}. \end{aligned} \tag{3.5}$$

Note that since $\sigma_1 = u^*_l - \frac{c_l}{\rho^*_l}$ and $\sigma_3 = u^*_r + \frac{c_r}{\rho^*_r}$, positivity of ρ is equivalent to $\sigma_1 < \sigma_2 < \sigma_3$.

3.2 Intermediate states for the 5-wave solver

A more general solver is obtained if we only set

$$b = 0, \tag{3.6}$$

and keep arbitrary c_a, c_b. Then we have the four parameters c_{bl}, c_{al}, c_{br}, c_{ar}. We observe that

$$c_s = \min(c_a, c_b), \qquad c_f = \max(c_a, c_b), \tag{3.7}$$

thus we have five eigenvalues for our system (2.1)–(2.8), which are $u - c_f/\rho$, $u - c_s/\rho$, u, $u + c_s/\rho$, $u + c_f/\rho$. The eigenvalues $u \pm c_a/\rho$ have double multiplicity, while $u \pm c_b/\rho$ are simple. We get a 5-wave solver with four intermediate states.

There are 8 strong Riemann invariants associated to the central wave (i.e. quantities that lie in the kernel of $\partial_t + u\partial_x$), which are c_a, c_b, b, and

$$\frac{1}{\rho} + \frac{\pi}{c_b^2}, \qquad \frac{B_\perp}{\rho} + \frac{B_x}{c_a^2}\pi_\perp, \qquad e + \frac{B_x^2 + |B_\perp|^2}{2\rho} - \frac{\pi^2}{2c_b^2} - \frac{|\pi_\perp|^2}{2c_a^2}. \tag{3.8}$$

These quantities are thus weak Riemann invariants for the other waves. Six weak Riemann invariants for the central wave are $u, u_\perp, \pi, \pi_\perp$. They take the same value on the

left and on the right of this central wave, we shall denote theses values by $u^*, u_\perp^*, \pi^*, \pi_\perp^*$. The remaining weak Riemann invariants for the left and right waves are found to be

$$\begin{aligned} &u - c_b/\rho : \pi + c_b u, \pi_\perp, u_\perp, \\ &u - c_a/\rho : \pi_\perp + c_a u_\perp, \pi, u, \\ &u + c_b/\rho : \pi - c_b u, \pi_\perp, u_\perp, \\ &u + c_a/\rho : \pi_\perp - c_a u_\perp, \pi, u. \end{aligned} \tag{3.9}$$

Therefore, everything is as if the longitudinal part of the velocity–pressure (u, π) were resolved independently of the transverse velocity–pressure $(u_\perp, \pi_\perp)$, the first jumping only through the c_b waves, and the second jumping only through the c_a waves. We deduce the values $u^*, u_\perp^*, \pi^*, \pi_\perp^*$ by replacing c by c_b or by c_a in (3.5),

$$\begin{aligned} u^* &= \frac{c_{bl} u_l + c_{br} u_r + \pi_l - \pi_r}{c_{bl} + c_{br}}, \\ \pi^* &= \frac{c_{br} \pi_l + c_{bl} \pi_r - c_{bl} c_{br} (u_r - u_l)}{c_{bl} + c_{br}}, \\ u_\perp^* &= \frac{c_{al} u_\perp^l + c_{ar} u_\perp^r + \pi_\perp^l - \pi_\perp^r}{c_{al} + c_{ar}}, \\ \pi_\perp^* &= \frac{c_{ar} \pi_\perp^l + c_{al} \pi_\perp^r - c_{al} c_{ar} (u_\perp^r - u_\perp^l)}{c_{al} + c_{ar}}. \end{aligned} \tag{3.10}$$

We complete the values of $u, \pi, u_\perp, \pi_\perp$ in the "noncentral" intermediate states by setting them to either their star value or their l/r value depending on the ordering between c_a and c_b. Indeed, if $c_b > c_a$ then $(u, \pi) = (u^*, \pi^*)$, $(u_\perp, \pi_\perp) = (u_\perp^{l/r}, \pi_\perp^{l/r})$, and if $c_b < c_a$ then $(u, \pi) = (u^{l/r}, \pi^{l/r})$, $(u_\perp, \pi_\perp) = (u_\perp^*, \pi_\perp^*)$.

The strong Riemann invariants (3.8) are constant on each side of the middle wave providing formulas for the intermediate values ρ, $B_\perp$ and e. In particular, ρ does not jump through the c_a waves.

Finally, we remark that u and π are given by u^* and π^* between the waves with speeds $u_l - \frac{c_{bl}}{\rho_l}$ and $u_r + \frac{c_{br}}{\rho_r}$, while there ρ takes the values ρ_l^* and ρ_r^*. The remaining left c_a wave hence has speed $u_l - \frac{c_{al}}{\rho_l}$ if $c_{al} \geq c_{bl}$, and $u^* - \frac{c_{al}}{\rho_{l*}}$ otherwise. The remaining right c_a wave has speed $u_r + \frac{c_{ar}}{\rho_r}$ if $c_{ar} \geq c_{br}$, and $u^* + \frac{c_{ar}}{\rho_{r*}}$ otherwise. Between these two c_a waves $u_\perp$ and $\pi_\perp$ are given by $u_\perp^*$ and $\pi_\perp^*$.

3.3 Previous 3-wave and 5-wave solvers

In [9,10] approximate Riemann solvers with 3 waves that resolve material contact discontinuities are given. No stability analysis is known in their case, and indeed instabilities can occur in practice. Miyoshi and Kusano proposed in [11] an approximate Riemann solver with 5 waves, that also accurately resolves Alfven contact waves. Even if no analysis of stability is provided, it is stable in practice.

3.4 Choice of signal speeds for the 3-wave solver

Here we derive explicit values for the signal speeds that are sufficient for positivity and entropy inequalities. This is done with the use of Proposition 2.1. Following the analysis of the classical gas dynamics case performed in [2], we make some natural assumptions on the pressure law, that is

$$\left(\frac{\partial}{\partial\rho}\right)_s \left(\rho\sqrt{p'}\right) > 0, \tag{3.11}$$

$$\left(\frac{\partial}{\partial\rho}\right)_s \left(\rho\sqrt{p'}\right) \leq \alpha\sqrt{p'}, \qquad \text{for some constant } \alpha > 1, \tag{3.12}$$

where we recall that p' is defined in (1.8). Notice that these assumptions only involve the pressure law $p(\rho)$ at fixed s, and that the first inequality is equivalent to p being convex with respect to $1/\rho$, at fixed s. For an ideal gas these conditions hold with $\alpha = \frac{1}{2}(\gamma+1)$. Considering now the 3-wave case, we make the following a priori choice of the relaxation speeds,

$$\begin{aligned} c_l &= \rho_l a_l^0 + \alpha\rho_l \left((u_l - u_r)_+ + \frac{(\pi_r - \pi_l)_+}{\rho_l a_{ql} + \rho_r a_{qr}}\right), \\ c_r &= \rho_r a_r^0 + \alpha\rho_r \left((u_l - u_r)_+ + \frac{(\pi_l - \pi_r)_+}{\rho_l a_{ql} + \rho_r a_{qr}}\right). \end{aligned} \tag{3.13}$$

Here, a_{ql}, a_{qr} denote the left and right fast MHD speeds,

$$a_q^2 = \frac{1}{2}\left(p' + \frac{B_x^2 + |B_\perp|^2}{\rho} + \sqrt{\left(p' + \frac{B_x^2 + |B_\perp|^2}{\rho}\right)^2 - 4p'\frac{B_x^2}{\rho}}\right), \tag{3.14}$$

and a_l^0 and a_r^0 need to be determined in such a way that

$$a_l^0 \geq a_{ql}, \qquad a_r^0 \geq a_{qr}. \tag{3.15}$$

This last restriction implies in particular that $c_l \geq \rho_l a_{ql}$, $c_r \geq \rho_r a_{qr}$. We would like now to find a value for a_l^0, such that $\rho_l^* > 0$, and that the conditions (2.17) of Proposition 2.1 are satisfied on the l^* state. From the first invariant of (3.2) we have that $1/\rho_l^* + \pi^*/c_l^2 = 1/\rho_l + \pi_l/c_l^2$, thus with the value of π^* given in (3.5),

$$\begin{aligned} \frac{1}{\rho_l^*} &= \frac{1}{\rho_l} + \frac{c_r(u_r - u_l) + \pi_l - \pi_r}{c_l(c_l + c_r)} \\ &\geq \frac{1}{\rho_l} - \frac{c_r(u_l - u_r)_+}{c_l(c_l + c_r)} - \frac{(\pi_r - \pi_l)_+}{c_l(c_l + c_r)} \\ &\geq \frac{1}{\rho_l} - \frac{(u_l - u_r)_+}{c_l} - \frac{(\pi_r - \pi_l)_+}{c_l(\rho_l a_{ql} + \rho_r a_{qr})}. \end{aligned} \tag{3.16}$$

Define now

$$X_l = \frac{1}{a_{ql}} \left((u_l - u_r)_+ + \frac{(\pi_r - \pi_l)_+}{\rho_l a_{ql} + \rho_r a_{qr}} \right), \tag{3.17}$$

so that by the definition (3.13) of c_l and by (3.15), one has

$$\frac{c_l}{\rho_l} \geq a_{ql}(1 + \alpha X_l). \tag{3.18}$$

Using this in (3.16) gives

$$\frac{1}{\rho_l^*} \geq \frac{1}{\rho_l} \left(1 - \frac{X_l}{1 + \alpha X_l} \right), \tag{3.19}$$

hence $\rho_l^* > 0$,

$$0 < \rho_l^* \leq \rho_l / x_l, \tag{3.20}$$

with

$$x_l = 1 - \frac{X_l}{1 + \alpha X_l} \quad \in \left(\frac{\alpha - 1}{\alpha}, 1 \right]. \tag{3.21}$$

The following Lemma generalizes the analysis performed for the Euler equations in [3].

Lemma 3.1 *Consider a pressure law $p(\rho)$ satisfying (3.11)–(3.12). Let $x = 1 - X/(1 + \alpha X)$ for some $X \geq 0$. Then for all $\rho > 0$*

$$\frac{\rho}{x} \sqrt{p' \left(\frac{\rho}{x} \right)} \leq \rho \sqrt{p'(\rho)} (1 + \alpha X). \tag{3.22}$$

Proof The assumptions imply that

$$\frac{d}{d\rho} \left(\rho^{-\alpha} \rho \sqrt{p'(\rho)} \right) \leq 0, \tag{3.23}$$

and thus that

$$\forall r \geq 1, \qquad r\rho \sqrt{p'(\rho)} \geq \rho r^{1/\alpha} \sqrt{p'(\rho r^{1/\alpha})}. \tag{3.24}$$

Taking $r = x^{-\alpha}$ gives

$$\frac{\rho}{x} \sqrt{p' \left(\frac{\rho}{x} \right)} \leq \rho \sqrt{p'(\rho)} x^{-\alpha}, \tag{3.25}$$

thus in order to conclude it only remains to prove that $x^{-\alpha} \leq 1+\alpha X$, or equivalently that $x \geq (1+\alpha X)^{-1/\alpha}$. This can be written

$$1 - \frac{X}{1+\alpha X} - (1+\alpha X)^{-1/\alpha} \geq 0. \tag{3.26}$$

Defining $\theta = 1/(1+\alpha X) \in [0,1]$, this reduces to

$$1 - \frac{1-\theta}{\alpha} - \theta^{1/\alpha} \geq 0, \tag{3.27}$$

which holds true for all $\theta \in [0,1]$ and $\alpha \geq 1$. □

Applying the lemma with $\rho = \rho_l$ gives

$$\frac{\rho_l}{x_l}\sqrt{p'\left(\frac{\rho_l}{x_l}, s_l\right)} \leq \rho_l \sqrt{p'(\rho_l, s_l)}(1+\alpha X_l). \tag{3.28}$$

According to the monotonicity of $\rho\sqrt{p'}$ stated in (3.11) and to (3.20), this allows to estimate the supremum of the speeds in (2.18),

$$\sqrt{(\rho^2 p')_{*,l}} \leq \rho_l \sqrt{p'_l}(1+\alpha X_l), \tag{3.29}$$

with $p'_l = p'(\rho_l, s_l)$. Now, in order to satisfy (2.17), it is sufficient to have

$$\left|B^l_\perp\right|^2 \leq \left(c_l^2 - \rho_l^2 p'_l (1+\alpha X_l)^2\right)\left(\frac{x_l}{\rho_l} - \frac{B_x^2}{c_l^2}\right), \tag{3.30}$$

provided that the two factors on the right-hand side are nonnegative. In order to simplify this, we write that $c_l = \rho_l(a_l^0 + \alpha a_{ql} X_l)$, thus

$$\begin{aligned} c_l^2 &= \rho_l^2\left((a_l^0)^2 + 2\alpha a_l^0 a_{ql} X_l + (\alpha a_{ql} X_l)^2\right) \\ &\geq \rho_l^2\left((a_l^0)^2 + 2\alpha a_{ql}^2 X_l + (\alpha a_{ql} X_l)^2\right). \end{aligned} \tag{3.31}$$

Therefore, we get

$$\begin{aligned} &c_l^2 - \rho_l^2 p'_l (1+\alpha X_l)^2 \\ &\quad \geq \rho_l^2\left((a_l^0)^2 - p'_l + 2\alpha X_l (a_{ql}^2 - p'_l) + (\alpha X_l)^2 (a_{ql}^2 - p'_l)\right) \\ &\quad \geq \rho_l^2\left((a_l^0)^2 - p'_l\right). \end{aligned} \tag{3.32}$$

Therefore, for (3.30) to hold it is enough that

$$\left|B_\perp^l\right|^2 \le \rho_l^2\left((a_l^0)^2 - p_l'\right)\left(\frac{x_l}{\rho_l} - \frac{B_x^2}{\rho_l^2(a_l^0)^2}\right), \tag{3.33}$$

provided that the two factors on the right-hand side are nonnegative. Multiplying this by $(a_l^0)^2$ we get a second degree inequality, and $(a_l^0)^2$ must be larger than its largest root. Therefore we can take for $(a_l^0)^2$ this largest root,

$$(a_l^0)^2 = \frac{1}{2}\left(p_l' + \frac{B_x^2 + |B_\perp^l|^2}{\rho_l x_l} + \sqrt{\left(p_l' + \frac{B_x^2 + |B_\perp^l|^2}{\rho_l x_l}\right)^2 - 4p_l'\frac{B_x^2}{\rho_l x_l}}\right). \tag{3.34}$$

Notice that this formula differs only by the appearance of x_l from the definition of a_{ql}. Since $x_l \le 1$, the condition $a_l^0 \ge a_{ql}$ in (3.15) holds true.

The same analysis is valid on the right, with

$$X_r = \frac{1}{a_{qr}}\left((u_l - u_r)_+ + \frac{(\pi_l - \pi_r)_+}{\rho_l a_{ql} + \rho_r a_{qr}}\right), \qquad x_r = 1 - \frac{X_r}{1 + \alpha X_r}, \tag{3.35}$$

$$(a_r^0)^2 = \frac{1}{2}\left(p_r' + \frac{B_x^2 + |B_\perp^r|^2}{\rho_r x_r} + \sqrt{\left(p_r' + \frac{B_x^2 + |B_\perp^r|^2}{\rho_r x_r}\right)^2 - 4p_r'\frac{B_x^2}{\rho_r x_r}}\right). \tag{3.36}$$

We have proved the following:

Proposition 3.2 *If the pressure law satisfies* (3.11)–(3.12)*, the 3-wave solver is positive and entropy satisfying for the choice of* c_l, c_r *given by* (3.13) *with* (3.34), (3.36), (3.17), (3.21), (3.35).

The above formulas are sharp in the sense that they give the true fast MHD speeds for constant initial data. Indeed, it is enough that $u_l = u_r$ and $\pi_l = \pi_r$ for getting $c_l = \rho_l a_{ql}$, $c_r = \rho_r a_{qr}$. This shows that fast waves are well resolved with this solver. Furthermore, one observes that with our choice of c_l, c_r, the maximum speed involved in the CFL condition (2.15) remains bounded when the speeds of the left and the right states are bounded, $(|u| + a_q)_{l/r} \le C$. This is true in particular if for example ρ_l approaches 0 with ρ_r fixed (but under the previous left/right bounds), as it was required in order to treat the vacuum in the Euler case, see [3].

3.5 Choice of signal speeds for the 5-wave solver

We here provide formulas for the signal speeds $c_{bl}, c_{br}, c_{al}, c_{ar}$ for the 5-wave solver that enable to get positivity and entropy inequalities. We still make the assumptions (3.11)–(3.12). In order to apply Proposition 2.1 we need that

$$\left|B_\perp^{l/r}\right|^2 \le \left(c_b^2 - (\rho^2 p')_{*,l/r}\right)\left(\frac{1}{\rho_*} - \frac{B_x^2}{c_a^2}\right), \tag{3.37}$$

with both factors on the right-hand side being nonnegative. If (3.37) is to hold sharply, a decrease in c_a implies an increase in c_b, and vice versa. In the 3-wave case we had $c_b = c_a$, and clearly that choice gives the least restrictive CFL-condition (2.15), where $c_f = \max(c_a, c_b)$ is involved. Another criterion for choosing c_a and c_b is to minimize the effect of the diffusion obtained from the Chapman–Enskog expansion. We shall make this choice here. The computation of the Chapman–Enskog expansion was performed in [5], and one can check that minimizing the largest eigenvalue of the diffusion matrix means minimizing $c_b^2 + c_a^2$. If we assume that (3.37) holds sharply (and for smooth solutions in the Chapman–Enskog context), minimum is achieved when

$$c_a^2 = \rho(B_x^2 + |B_x B_\perp|), \quad \text{and} \quad c_b^2 = \rho^2 p' + \rho(|B_\perp|^2 + |B_x B_\perp|). \tag{3.38}$$

Then, for this choice, the largest eigenvalue of the diffusion matrix is $2|B_x B_\perp|/\rho$. We notice that it implies that the diffusion matrix vanishes identically when $B_x = 0$ or $B_\perp = 0$. The case when $B_x = 0$ or $B_\perp = 0$ means that two eigenvalues of the MHD system coincide (the system has at most 5 waves instead of 7). Therefore, it means that whenever the MHD system has at most 5 waves, the 5-wave solver with the choice (3.38) becomes fully accurate (it has only the residual viscosity due to averaging on the cells, or equivalently it has the same viscosity as the exact Godunov scheme).

We would like now to make a choice of c_{al}, c_{bl}, c_{ar}, c_{br} for our solver in such a way that for constant data we obtain the values (3.38). In order to analyze the stability conditions, we notice that the intermediate densities are given by a formula similar to the 3-wave case,

$$\frac{1}{\rho_l^*} = \frac{1}{\rho_l} + \frac{c_{br}(u_r - u_l) + \pi_l - \pi_r}{c_{bl}(c_{bl} + c_{br})}, \qquad \frac{1}{\rho_r^*} = \frac{1}{\rho_r} + \frac{c_{bl}(u_r - u_l) + \pi_r - \pi_l}{c_{br}(c_{bl} + c_{br})}. \tag{3.39}$$

This suggests to take c_{bl}, c_{br} similarly as in (3.13),

$$\begin{aligned} c_{bl} &= \rho_l a_l^0 + \alpha\rho_l \left((u_l - u_r)_+ + \frac{(\pi_r - \pi_l)_+}{\rho_l a_{bql} + \rho_r a_{bqr}} \right), \\ c_{br} &= \rho_r a_r^0 + \alpha\rho_r \left((u_l - u_r)_+ + \frac{(\pi_l - \pi_r)_+}{\rho_l a_{bql} + \rho_r a_{bqr}} \right), \end{aligned} \tag{3.40}$$

but now with a_{bql}, a_{bqr} defined by

$$a_{bq}^2 = p' + \frac{|B_\perp|^2 + |B_x B_\perp|}{\rho}. \tag{3.41}$$

We look for values a_l^0, a_r^0 satisfying

$$a_l^0 \geq a_{bql}, \qquad a_r^0 \geq a_{bqr}. \tag{3.42}$$

This restriction implies in particular that $c_{bl} \geq \rho_l a_{bql}$, $c_{br} \geq \rho_r a_{bqr}$. Then, we set

$$X_l = \frac{1}{a_{bql}} \left((u_l - u_r)_+ + \frac{(\pi_r - \pi_l)_+}{\rho_l a_{bql} + \rho_r a_{bqr}} \right), \tag{3.43}$$

so that by (3.40) and (3.42), one has

$$\frac{c_{bl}}{\rho_l} \geq a_{bql}(1 + \alpha X_l). \tag{3.44}$$

Estimating the density ρ_l^* given in (3.39) similarly as in (3.16) yields that

$$0 < \rho_l^* \leq \rho_l / x_l, \tag{3.45}$$

with

$$x_l = 1 - \frac{X_l}{1 + \alpha X_l} \quad \in \left(\frac{\alpha - 1}{\alpha}, 1 \right]. \tag{3.46}$$

Now we observe that we have two intermediate states on the left, but however for any of them, its density ρ^* is equal either to ρ_l^*, or to ρ_l. Thus $\rho^* > 0$, and

$$\sup_{\rho \in [\rho^*, \rho_l]} \rho \leq \frac{\rho_l}{x_l}. \tag{3.47}$$

Therefore, according to the monotonicity of $\rho\sqrt{p'}$ stated in (3.11), the maximal speed in (2.18) can be estimated as

$$\sqrt{(\rho^2 p')_{*,l}} \leq \frac{\rho_l}{x_l} \sqrt{p' \left(\frac{\rho_l}{x_l}, s_l \right)} \leq \rho_l \sqrt{p_l'} (1 + \alpha X_l), \tag{3.48}$$

the latter inequality resulting from Lemma 3.1. Thus, in order to get (3.37), it is enough that

$$\left| B_\perp^l \right|^2 \leq \left(c_{bl}^2 - \rho_l^2 p_l' (1 + \alpha X_l)^2 \right) \left(\frac{x_l}{\rho_l} - \frac{B_x^2}{c_{al}^2} \right), \tag{3.49}$$

provided that the two factors on the right-hand side are nonnegative. Next, we write $c_{bl} = \rho_l (a_l^0 + \alpha a_{bql} X_l)$, and the same estimates as in (3.31)–(3.32) give

$$c_{bl}^2 - \rho_l^2 p_l' (1 + \alpha X_l)^2 \geq \rho_l^2 \left((a_l^0)^2 - p_l' \right). \tag{3.50}$$

Therefore, for (3.49) to hold it is sufficient to have

$$\left| B_\perp^l \right|^2 \leq \rho_l^2 \left((a_l^0)^2 - p_l' \right) \left(\frac{x_l}{\rho_l} - \frac{B_x^2}{c_{al}^2} \right), \tag{3.51}$$

with the two factors on the right-hand side being nonnegative. Our choice is then to take

$$(a_l^0)^2 = p_l' + \frac{|B_\perp^l|^2 + |B_x B_\perp^l|}{\rho_l x_l}, \tag{3.52}$$

$$c_{al}^2 = \frac{\rho_l}{x_l}\left(B_x^2 + |B_x B_\perp^l|\right), \tag{3.53}$$

that gives equality in (3.51). Since $x_l \le 1$ the condition that $a_l^0 \ge a_{bql}$ in (3.42) is satisfied. Notice again that (3.52) differs only by the factor $1/x_l$ from the definition of a_{bql}.

A similar analysis on the right leads to

$$X_r = \frac{1}{a_{bqr}}\left((u_l - u_r)_+ + \frac{(\pi_l - \pi_r)_+}{\rho_l a_{bql} + \rho_r a_{bqr}}\right), \qquad x_r = 1 - \frac{X_r}{1 + \alpha X_r}, \tag{3.54}$$

$$(a_r^0)^2 = p_r' + \frac{|B_\perp^r|^2 + |B_x B_\perp^r|}{\rho_r x_r}, \qquad c_{ar}^2 = \frac{\rho_r}{x_r}\left(B_x^2 + |B_x B_\perp^r|\right). \tag{3.55}$$

We have proved the following:

Proposition 3.3 *If the pressure law satisfies* (3.11)–(3.12)*, the 5-wave solver is positive and entropy satisfying for the choice of* c_{bl}*,* c_{br}*,* c_{al}*,* c_{ar} *given by* (3.40)*,* (3.52)*,* (3.53)*,* (3.43)*,* (3.46)*,* (3.54)*,* (3.55)*.*

As it was chosen, for constant data the values of c_a, c_b reduce to (3.38), hence the solver becomes fully accurate whenever B_x or $B_\perp$ vanishes (or is sufficiently small). Thus, an interest of this 5-wave solver is to be able to use it as a "patch" for other solvers using 7 waves, that may have singularities when two eigenvalues become too close.

However, a weak point in our 5-wave solver is that its maximal wave speed $c_f/\rho = \max(c_a/\rho, c_b/\rho)$ involved in the CFL condition (2.15) exceeds the maximal speed of the MHD system, which is a_q in (3.14). This excess can be evaluated by the ratios $c_a/\rho a_q$ and $c_b/\rho a_q$, where c_a, c_b are given in (3.38). For the first one, studying the variations with respect to p' one can easily prove that

$$\frac{c_a}{\rho a_q} = \sqrt{\frac{B_x^2 + |B_x B_\perp|}{\rho a_q^2}} \le \sqrt{\frac{1}{2} + \sqrt{\frac{1}{2}}} \approx 1.099. \tag{3.56}$$

For the second it is not so easy, but with the same method we get the same upper bound

$$\frac{c_b}{\rho a_q} = \sqrt{\frac{p'}{a_q^2} + \frac{|B_\perp|^2 + |B_x B_\perp|}{\rho a_q^2}} \le \sqrt{\frac{1}{2} + \sqrt{\frac{1}{2}}}. \tag{3.57}$$

This implies that the overall computational cost can be only of 10% in the worst case. In practice the 5-wave solver uses timesteps close to what the 3-wave solver uses.

4 Numerical tests

In this section we investigate the accuracy and robustness in numerical computations of the relaxation-based Riemann solvers with 3 and 5 waves. We compare them with each other and with other methods. In all cases we use the solvers in the first-order Godunov scheme (2.12). In order to get reference solutions we performed high resolution computations with the entropy satisfying 3-wave solver. The CFL-number was 0.9 in all tests. We summarize the Riemann initial data taken as test cases in Table 1. Note that we use the notation $u_\perp = (v, w)$ and $B_\perp = (B_y, B_z)$.

For comparison purposes we consider the Roe solver of [1], the HLL solver, and the 5-wave solver of [11], denoted by MK5. As signal speeds for HLL and MK5 we used the speeds for the 3-wave solver from Sect. 3. For the HLL solver this choice ensures positivity and entropy inequalities. This is because if we consider the conserved quantities, the intermediate value of the HLL solver is equal to the spatial average between the intermediate states of the 3-wave solver. Hence positivity of density and internal energy is inherited by convex combination, and entropy inequalities are obtained via Jensen's inequality.

Table 1 Table of initial data for shock tube tests

Test	ρ	u	v	w	p	B_x	B_y	B_z	γ
Dai-Woodward left	1.08	1.2	0.01	0.5	0.95	$\frac{4}{\sqrt{4\pi}}$	$\frac{3.6}{\sqrt{4\pi}}$	$\frac{2}{\sqrt{4\pi}}$	$\frac{5}{3}$
Dai-Woodward right	1.0	0.0	0.0	0.0	1.0	$-\,\shortparallel\,-$	$\frac{4}{\sqrt{4\pi}}$	$\frac{2}{\sqrt{4\pi}}$	$-\,\shortparallel\,-$
Brio-Wu I left	1.0	0.0	0.0	0.0	1.0	0.75	1.0	0.0	2.0
Brio-Wu I right	0.125	0.0	0.0	0.0	0.1	$-\,\shortparallel\,-$	-1.0	0.0	$-\,\shortparallel\,-$
Brio-Wu II left	1.0	0.0	0.0	0.0	1000.0	0.0	1.0	0.0	2.0
Brio-Wu II right	0.125	0.0	0.0	0.0	0.1	$-\,\shortparallel\,-$	-1.0	0.0	$-\,\shortparallel\,-$
Slow rarefaction left	1.0	0.0	0.0	0.0	2.0	1.0	0.0	0.0	$\frac{5}{3}$
Slow rarefaction right	0.2	1.186	2.967	0.0	0.1368	$-\,\shortparallel\,-$	1.6405	0.0	$-\,\shortparallel\,-$
Vacuum problem left	0.0	0.0	0.0	0.0	0.0	0.0	0.0	0.0	2
Vacuum problem right	1.0	0.0	0.0	0.0	0.5	$-\,\shortparallel\,-$	1.0	0.0	$-\,\shortparallel\,-$
Expansion problem left	1.0	-3.1	0.0	0.0	0.45	0.0	0.5	0.0	$\frac{5}{3}$
Expansion problem right	1.0	3.1	0.0	0.0	0.45	$-\,\shortparallel\,-$	0.5	0.0	$-\,\shortparallel\,-$
Expansion problem II left	1.0	-3.1	0.0	0.0	0.45	1.0	0.5	0.0	$\frac{5}{3}$
Expansion problem II right	1.0	3.1	0.0	0.0	0.45	$-\,\shortparallel\,-$	0.5	0.0	$-\,\shortparallel\,-$

4.1 Shock tube of Dai and Woodward

This shock tube test was introduced in [7]. The initial data are given as 'Dai–Woodward' in Table 1. The solution consists of shocks and contact discontinuities for all characteristic fields. On this test we compare our solvers against the Roe solver of [1]. This particular Roe solver, based on entropy variables, seems to give very sharp resolution. For the Roe solver we used a CFL number of 0.45, since it is unstable for values too close to 1. It gives the expected high accuracy on this fairly mild test case,

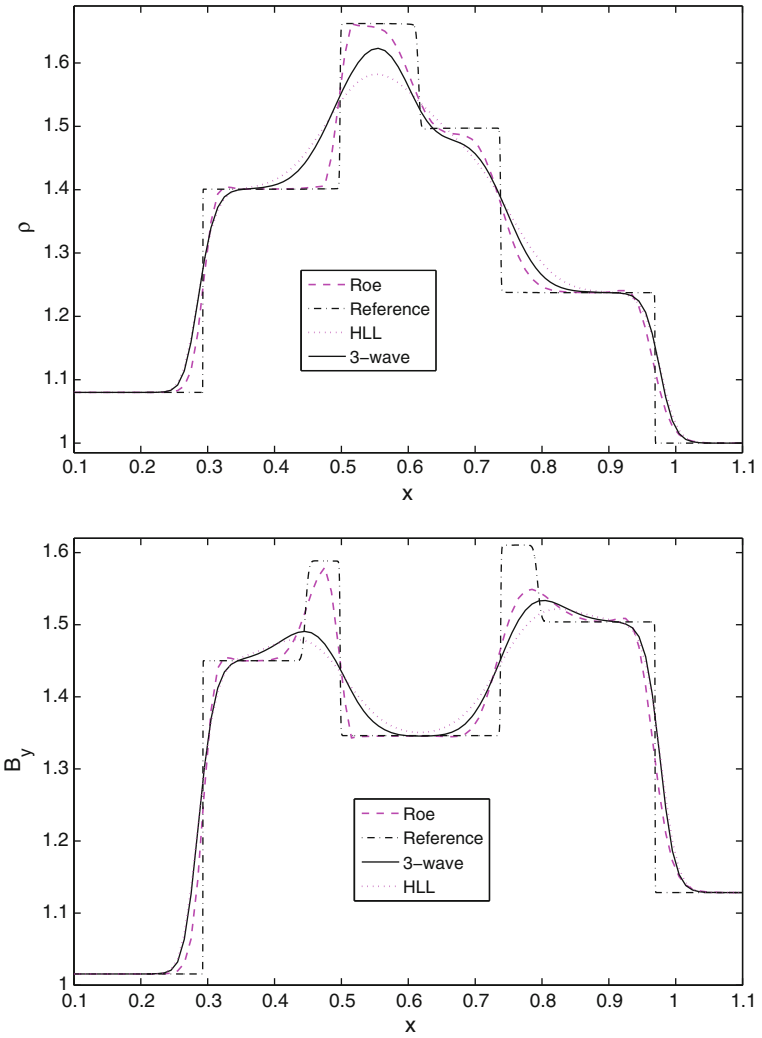

Fig. 1 ρ and B_y for Dai–Woodward shock tube at time $t = 0.2$ with resolution $\Delta x = 0.01$. The reference solution is a 3-wave simulation with $\Delta x = \frac{2}{3}10^{-4}$

see Fig. 1. We also note that the 3-wave solver gives a much better resolution than HLL, especially of the density ρ. The 5-wave solver performs similarly to the 3-wave solver except that it slightly improves the resolution of the left-going Alfven wave.

In Fig. 2 we compare our 3-wave solver to the MK5 solver. As signal speeds in the MK5 solver we used our speeds for the 3-wave solver. For that reason it is not surprising that the performance on fast waves differ very little. At the left-going Alfven and slow waves MK5 is sharper than with our 3- and 5-wave solvers.

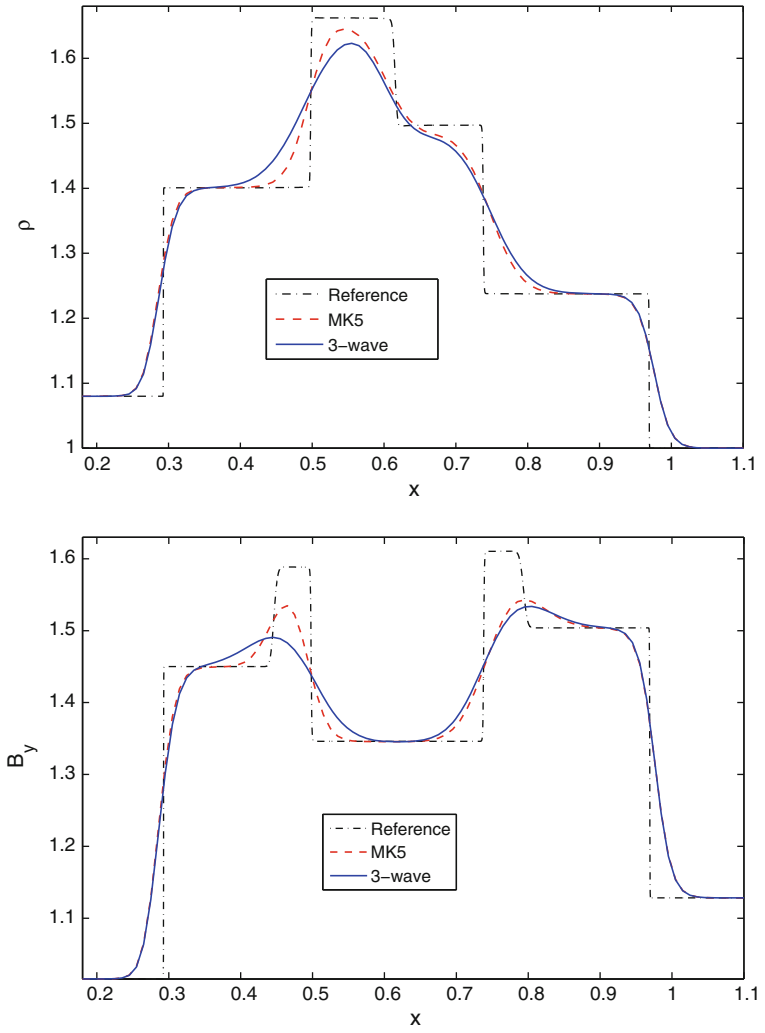

Fig. 2 ρ and B_y for Dai–Woodward shock tube at time $t = 0.2$ with resolution $\Delta x = 0.01$. The reference solution is a 3-wave simulation with $\Delta x = \frac{2}{3}10^{-4}$

4.2 Brio–Wu shock tube I

Next we consider the shock tube tests of [6], denoted by 'Brio–Wu I'. Figure 3 shows the resulting ρ and B_y. The solution consists of, from left to right, a fast rarefaction, a compound wave, a contact discontinuity, and a slow shock. The compound wave is a discontinuity attached to a slow rarefaction, it can be attributed to the non strict hyperbolicity of the system (1.1)–(1.5). There is also a small Alfven wave and a fast rarefaction going to the right, that are not shown in Fig. 3. We first compare our 3-wave solver with the HLL solver. As expected the 3-wave solver has much better

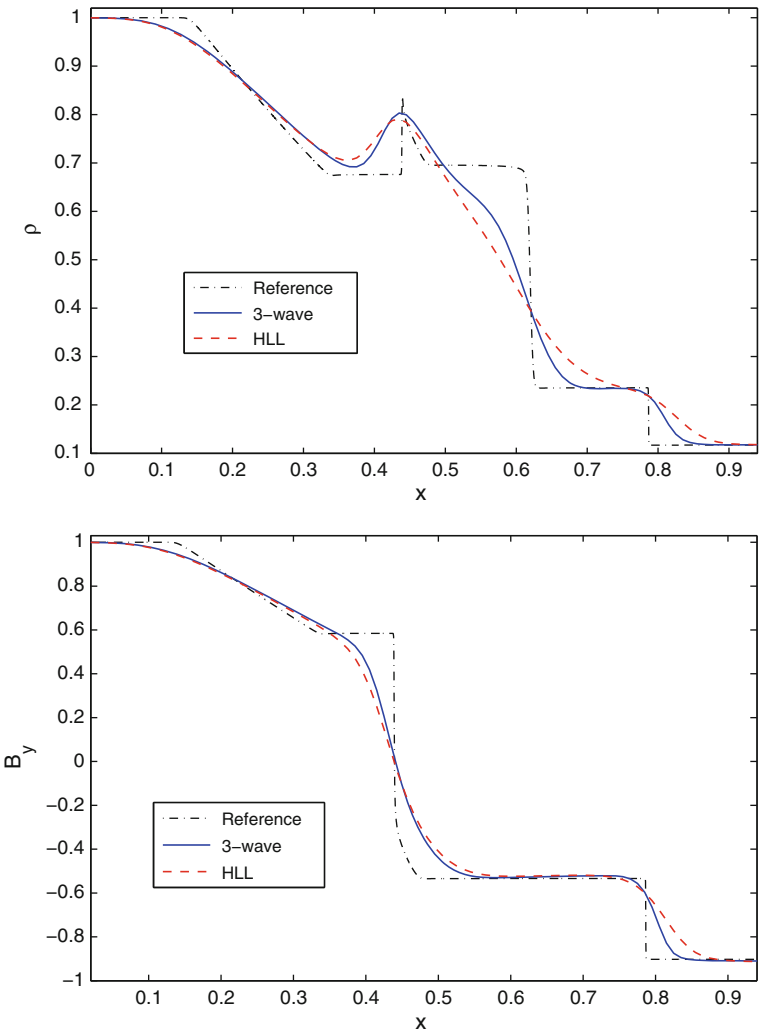

Fig. 3 ρ and B_y for Brio–Wu shock tube I at time $t = 0.2$ with resolution $\Delta x = 0.01$. The reference solution is a 3-wave simulation with $\Delta x = 0.0001$

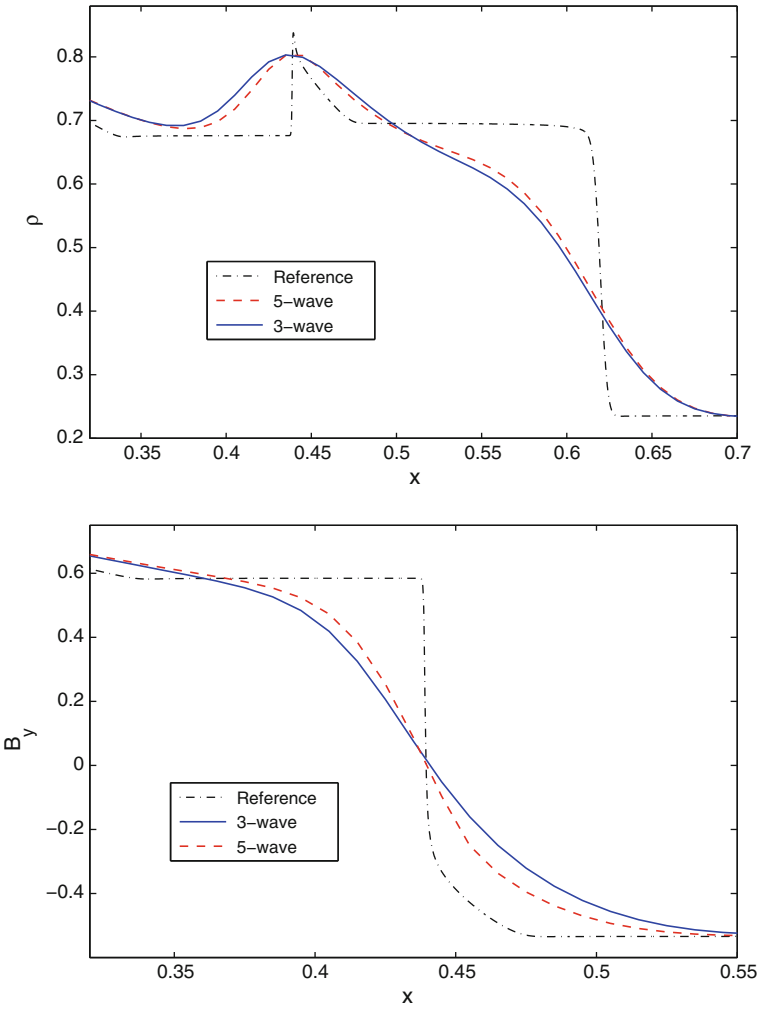

Fig. 4 ρ and B_y for Brio–Wu shock tube I at time $t = 0.2$ with resolution $\Delta x = 0.01$. The reference solution is a 3-wave simulation with $\Delta x = 0.0001$

resolution of the contact discontinuity. Figure 3 shows that the 3-wave solver also strongly improves the sharpness of the slow shock and the compound wave. The fast waves are well resolved by both solvers. We also see that the 5-wave solver gives good results on these waves. Figure 4 shows that the 5-wave solver improves the resolution of the compound wave compared to the 3-wave solver. This has to do with $B_\perp$ being locally small.

4.3 Brio–Wu shock tube II

The second test from [6] is a case with high fast magnetosonic Mach number. Since $B_x = 0$, and $u_\perp = 0$, the 3-, 5-wave and MK5 solvers are identical, and a full 7-wave

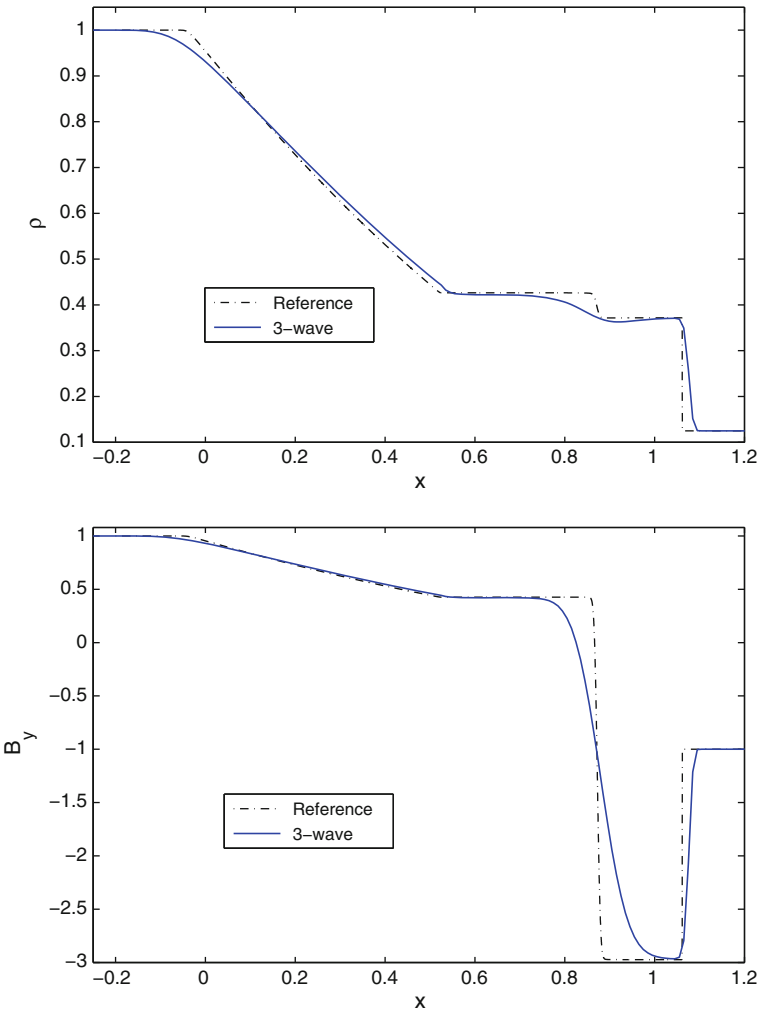

Fig. 5 ρ and B_y for Brio–Wu shock tube II at time $t = 0.012$ with resolution $\Delta x = 0.01$. The reference solution is a 3-wave simulation with $\Delta x = 0.0001$. The 3- and 5-wave solvers are the same in this case

solver cannot be expected to perform better. The results are shown in Figure 5. In this case we do not gain much compared to HLL from exactly resolving the contact wave, since it moves much faster than the magnetosonic speeds. The smearing of the contact wave is mostly due to numerical diffusion inherent in the Godunov scheme. Both fast waves are reasonably well resolved.

4.4 Shear waves

This example illustrates the numerical accuracy on Alfven waves of the different solvers. We choose the initial data

$$\rho = 1.0, \quad p = 1.0, \quad u = 1.0,$$
$$B_y = \sin(2\pi x), \quad B_z = \cos(2\pi x),$$
$$v = \sin(2\pi x), \quad w = \cos(2\pi x),$$
$$B_x = 1.0, \quad \gamma = 5/3.$$

This specifies a stationary left Alfven wave. We expect that the 5-wave solver will give a better approximation than the 3-wave, and this is confirmed by the plot of B_y in Fig. 6. We also made the same computation with $p = 100.0$, which still gives a stationary Alfven wave. In this case the 5-wave solver is superior as expected, as Fig. 7 shows. We also note in Figs. 6, 7 that the 3-wave solver is a clear improvement with respect to the HLL solver.

4.5 Slow sonic rarefaction

This test is a slow switch-on rarefaction suggested in [8], and also used in [11]. The data are given in Table 1 There is a sonic point in this rarefaction, that is a point where slow magnetosonic speed equals the fluid velocity. A linearized solver will typically produce an unphysical shock at the sonic point unless additional numerical diffusion is added. Figure 8 shows that the 3-wave solver is able to handle this problem in a stable manner with good accuracy. It gives an improvement with respect to the HLL solver. The structures in the density profile behind the rarefaction can be referred to as start-up errors, and these are basically unavoidable for certain kinds of Riemann problems. The 5-wave solver gives slightly better results than the 3-wave solver for the magnetic field B_y, otherwise they are practically the same.

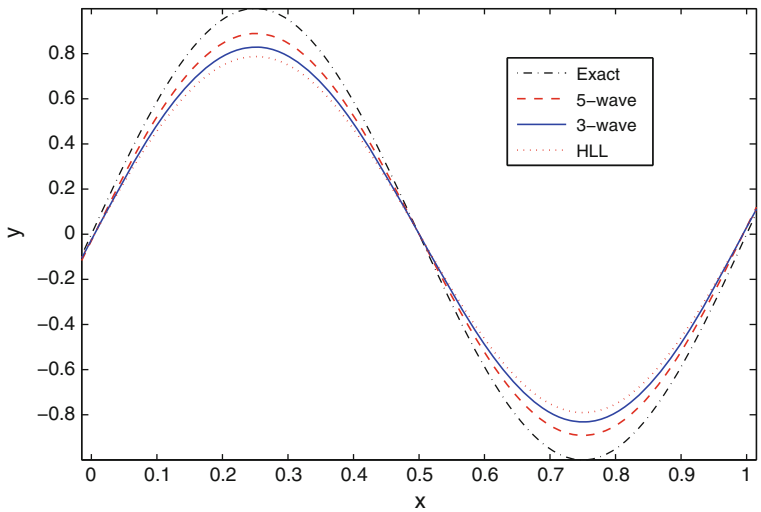

Fig. 6 B_y for a smooth Alfven wave with resolution $\Delta x = 0.01$ at time $t = 1.0$

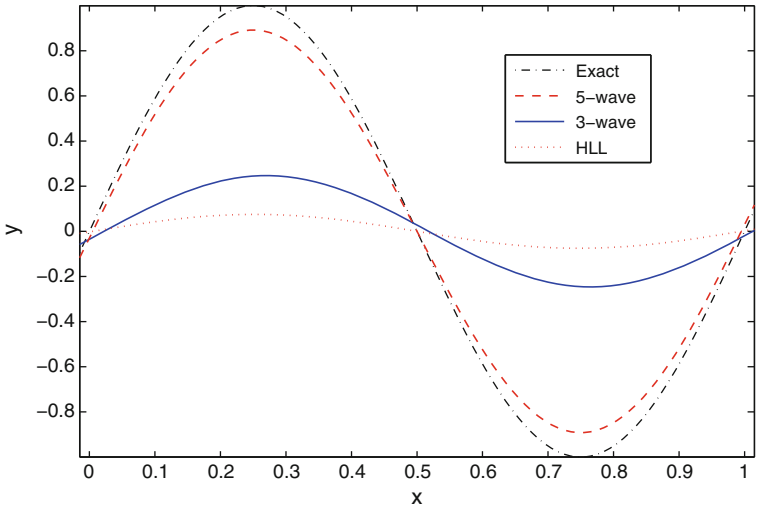

Fig. 7 The same as in Figure 6, but with pressure 100 times higher

4.6 Vacuum problem

An interesting test for the stability of a scheme is how it handles a Riemann problem where one initial state is vacuum (see [2,3]). In the case of ideal MHD we have to take zero magnetic field in the vacuum region to keep the characteristic speeds finite. This implies that $B_x = 0$ everywhere. Since also $u_\perp = 0$ in our case, the 3- and 5-wave solvers are the same. Consider a vacuum left state with $\rho_l = 0$, $\mathbf{B}_l = 0$, and a right state with $\rho_r > 0$, $p_r > 0$. Then, c_l, c_r and the intermediate states are well defined. We assume in order to get a value for c_l/ρ_l that $\mathbf{B}_l/\sqrt{\rho_l} = 0$. Note that no quantities jump across the left-going wave. Therefore, the quantity c_l/ρ_l is only used in calculating the CFL condition. Furthermore, its contribution to the CFL condition is not strictly needed.

In the case when $\gamma = 2$ (i.e. $p = \rho e$), and $B_z = 0$, we can write the solution as $B_y = \frac{B_y^r}{\rho_r}\rho$, together with a pure Euler system written in terms of ρ, u and an auxiliary internal energy $\widetilde{e} = e + \frac{1}{2}\rho\left(\frac{B_y^r}{\rho_r}\right)^2$. Then, since a rarefaction wave is isentropic, we get the classical solution

$$
\begin{aligned}
u(t,x) &= \frac{2}{3}\left(\max\left(\frac{x-\frac{1}{2}}{t}, -2\sqrt{2\widetilde{e}_r}\right) - \sqrt{2\widetilde{e}_r}\right)_-, \\
\rho(t,x) &= \rho_r\left(1 + \frac{1}{2}\frac{u(t,x)}{\sqrt{2\widetilde{e}_r}}\right)_+^2, \\
\widetilde{e}(t,x) &= \rho(t,x)\frac{\widetilde{e}_r}{\rho_r}.
\end{aligned}
\tag{4.1}
$$

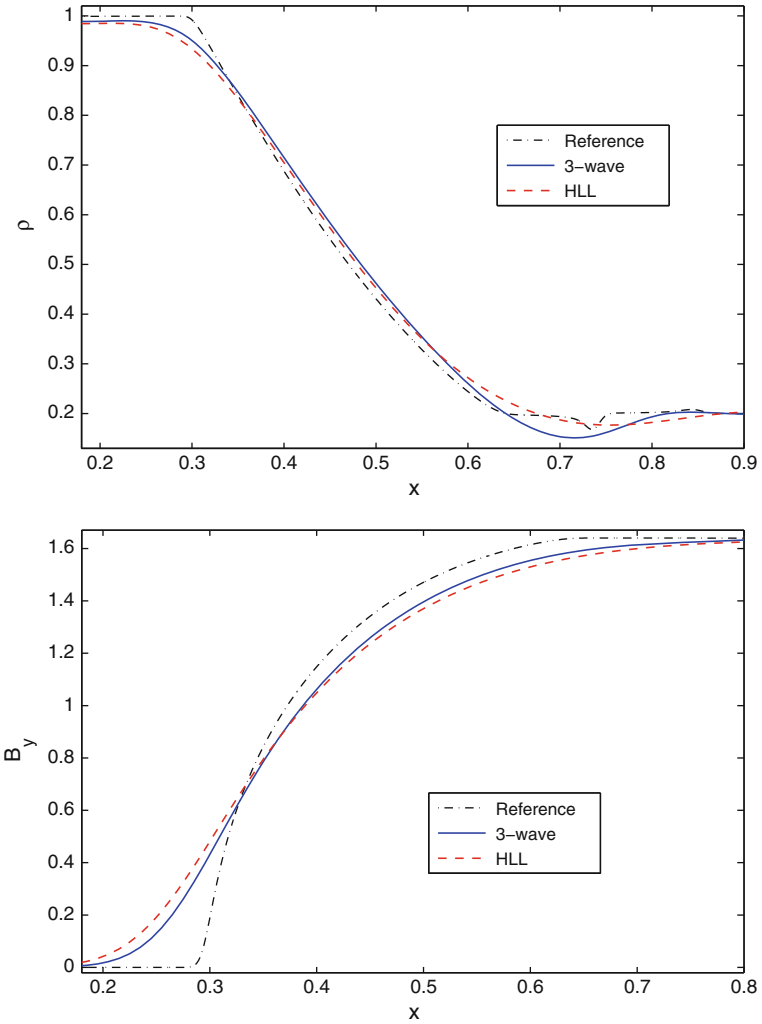

Fig. 8 Slow rarefaction at time $t = 0.2$ with resolution $\Delta x = 0.01$. The reference solution is a 3-wave simulation with $\Delta x = 0.0002$

The Figs. 9–10 show that our solver handles this vacuum test case well. The MK5 solver with our 3-wave speeds is identical to the 3-wave solver in this case ($u_\perp = 0$, $B_x = 0$), and hence would give the same result.

4.7 Expansion problem

This test is from [11]. It consists of two rarefactions separating a low density region, which is difficult to compute, especially for linearized solvers. Since $B_x = 0$ and $u_\perp = 0$, the 3- , 5-wave and MK5 solvers are the same, as in Sect. 4.3. HLL with the same signal speeds as the 3-wave solver does an equally good job as the 3-wave

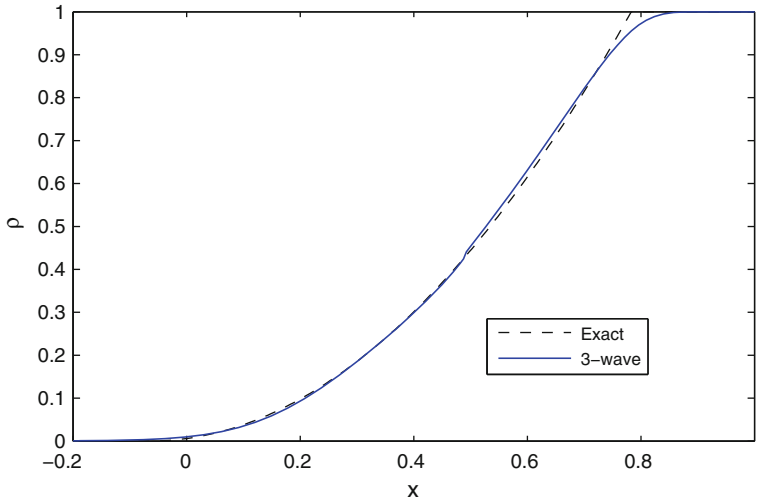

Fig. 9 Vacuum problem at time $t = 0.2$ with resolution $\Delta x = 0.005$. The 3- and 5-wave solvers are the same in this case

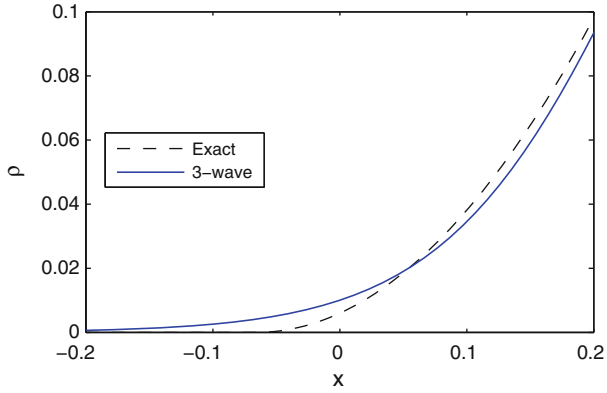

Fig. 10 Vacuum problem at time $t = 0.2$ with resolution $\Delta x = 0.005$. The 3- and 5-wave solvers are the same in this case

solver. Figure 11 shows ρ computed with the 3-wave solver. This is a good result as one would expect.

4.8 Low thermal pressure

Taking B_x nonzero in the above example causes $\frac{\rho p'}{|B|^2}$ to become small in the center region in the wake of two strong slow rarefactions. This is an additional difficulty to the low density and pressure. The 3-wave and 5-wave solvers both handle this case well, and give almost identical results. They resolve the density better than HLL, as

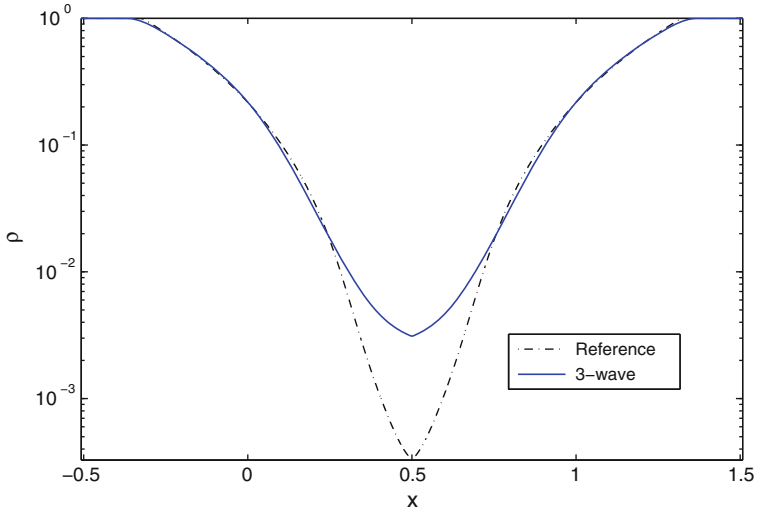

Fig. 11 Expansion problem at time $t = 0.2$ with resolution $\Delta x = 0.005$. Note the logarithmic y-axis. The reference solution is a 3-wave simulation with $\Delta x = 0.0002$. The 3- and 5-wave solvers are the same in this case

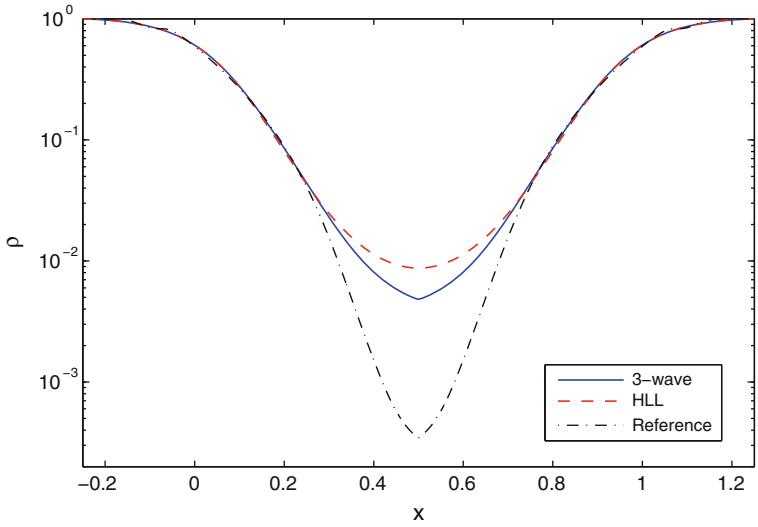

Fig. 12 Expansion problem with $B_x = 1.0$ at time $t = 0.15$ with resolution $\Delta x = 0.005$. Note the logarithmic y-axis. The reference solution is a 3-wave simulation with $\Delta x = \frac{2}{3}10^{-4}$

seen from Fig. 12. The magnetic field B_y is shown in Fig. 13, and for that quantity there is less difference between the codes.

We also plotted $\beta = 2\frac{p}{|B|^2}$, see Figure 14. The low values make this an interesting test case. In Figure 15 we compare our solvers with the MK5 solver. We notice that the latter gives similar results to the 3-wave solver, while our 5-wave solver computes the

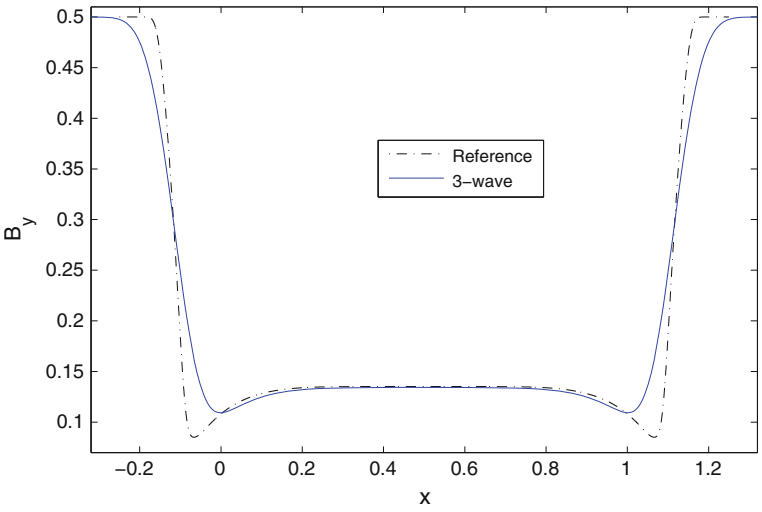

Fig. 13 Expansion problem with $B_x = 1.0$ at time $t = 0.15$ with resolution $\Delta x = 0.005$

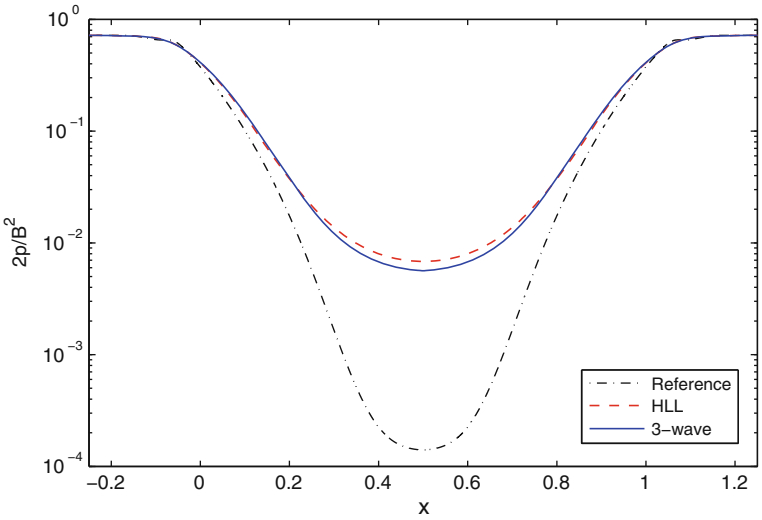

Fig. 14 Expansion problem with $B_x = 1.0$ at time $t = 0.15$ with resolution $\Delta x = 0.005$. Note the logarithmic y-axis. The figure shows the ratio of thermal and magnetic pressure

thermal pressure more accurately. The specific internal energy reaches its maximum $e_{\max}$ at $x = 0.5$ in all cases. With our 5-wave solver we get $e_{\max} = 0.698$, while the MK5 gives $e_{\max} = 1.121$, which is a significant difference. The reference solution has $e_{\max} = 0.310$. Note that the quantity e is proportional to the temperature for an ideal gas.

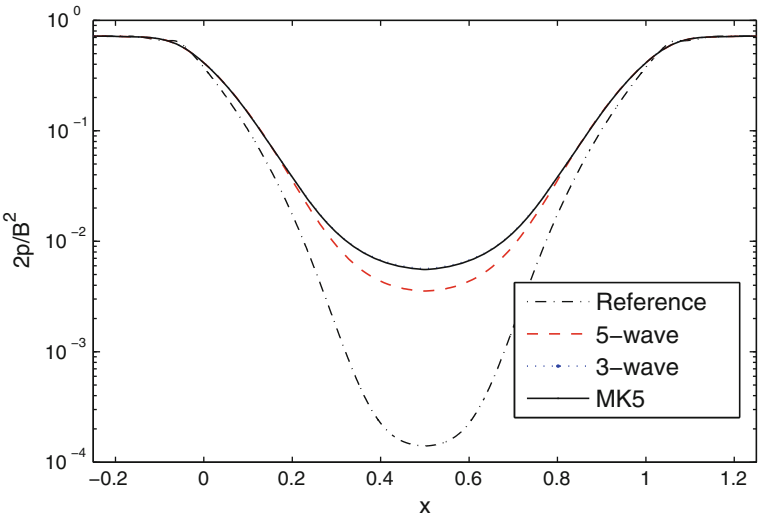

Fig. 15 Expansion problem with $B_x = 1.0$ at time $t = 0.15$ with resolution $\Delta x = 0.005$. Note the logarithmic y-axis. The reference solution is a 3-wave simulation with $\Delta x = \frac{2}{3}10^{-4}$

4.9 Conclusion

We summarize the results from this section in the following points.

- The 3-wave solver resolves slow moving contacts much better than HLL.
- The 3-wave solver also improves the resolution of Alfven waves and slow waves compared to HLL.
- The 3-and 5-wave solvers can handle rarefactions into low density and low $\beta = 2\frac{p}{|B|^2}$.
- The 5-wave solver can, in contrast to the 3-wave solver, sharply resolve all waves when B_x or $B_\perp$ vanishes.
- The 5-wave solver is significantly sharper on Alfven waves in certain regimes. In particular when Alfven speed is smaller than sound speed, or when $|B_x|$ is smaller than $|B_\perp|$. This appears from the numerical tests to also be the case for the slow modes in certain cases.

The 3- and 5-wave solvers are ready to be applied on physical problems. They provide good accuracy and excellent stability properties, with simple and explicit formulas. In most cases, the 3-wave solver should perform better, because it runs faster. It also allows larger timesteps, although the difference is not really significant. At high β though, the 5-wave solver is much less diffusive. This is also the case if one has a strong grid-aligned magnetic field.

5 Appendix: Powell's system

In this appendix we propose a method to numerically deal with nonconstant B_x. This can be useful when dealing with multidimensional MHD and the $\operatorname{div}\mathbf{B} = 0$ constraint. We shall denote here $\mathbf{B} = (B_x, B_\perp)$ and $\mathbf{u} = (u, u_\perp)$.

Following Powell [12], the so called Powell system in three dimensions (indeed one of its versions) is obtained by removing the constraint $\operatorname{div}\mathbf{B} = 0$ in the MHD system and by adding a term $\mathbf{u}\operatorname{div}\mathbf{B}$ on the induction equation, leading to

$$\begin{aligned}
&\rho_t + \operatorname{div}(\rho\mathbf{u}) = 0,\\
&(\rho\mathbf{u})_t + \operatorname{div}\left(\rho\mathbf{u}\otimes\mathbf{u} + \left(p + \frac{1}{2}|\mathbf{B}|^2\right)\operatorname{Id} - \mathbf{B}\otimes\mathbf{B}\right) = 0,\\
&E_t + \operatorname{div}\left[\left(E + p + \frac{1}{2}|\mathbf{B}|^2\right)\mathbf{u} - (\mathbf{B}\cdot\mathbf{u})\mathbf{B}\right] = 0,\\
&\mathbf{B}_t + \operatorname{div}(\mathbf{B}\otimes\mathbf{u} - \mathbf{u}\otimes\mathbf{B}) + \mathbf{u}\operatorname{div}\mathbf{B} = 0,
\end{aligned} \tag{5.1}$$

where E is still given by (1.6). This system is a classical quasilinear system, and only the induction equation is not in conservative form. Some of the main properties of Powell's system are:

1. Powell's system is hyperbolic, its eigenvalues being given by the same formulas as for the MHD system, the only difference being that u has now multiplicity 2,
2. Under the assumptions (1.7), (1.8), (1.9), Powell's system has the same entropy inequalities as the classical MHD system

$$(\rho\phi(s))_t + \operatorname{div}(\rho\phi(s)\mathbf{u}) \le 0, \tag{5.2}$$

   for all nonincreasing convex ϕ,
3. Solutions to Powell's system such that $\operatorname{div}\mathbf{B} \equiv 0$ are solutions to the MHD system,
4. Solutions to Powell's system such that $\operatorname{div}\mathbf{B}(0,x) \equiv 0$ satisfy also $\operatorname{div}\mathbf{B}(t,x) \equiv 0$ for all times t, because one has

$$(\operatorname{div}\mathbf{B})_t + \operatorname{div}(\mathbf{u}\operatorname{div}\mathbf{B}) = 0. \tag{5.3}$$

Thus such solutions are also solutions to the MHD system (1.1)–(1.5).

5.1 Powell's system in one dimension

In one space dimension, Powell system reads

$$\begin{aligned}
&\rho_t + (\rho u)_x = 0,\\
&(\rho u)_t + \left(\rho u^2 + p + \frac{1}{2}|B_\perp|^2 - \frac{1}{2}B_x^2\right)_x = 0,\\
&(\rho u_\perp)_t + (\rho u u_\perp - B_x B_\perp)_x = 0,\\
&E_t + \left[\left(E + p + \frac{1}{2}|B_\perp|^2 - \frac{1}{2}B_x^2\right)u - B_x(B_\perp \cdot u_\perp)\right]_x = 0,\\
&(B_x)_t + u(B_x)_x = 0,\\
&(B_\perp)_t + (B_\perp u - B_x u_\perp)_x + u_\perp (B_x)_x = 0.
\end{aligned} \tag{5.4}$$

Instead of being constant previously, B_x is now advected at velocity u. Note that the nonconservative products in the induction equations do not induce any difficulty concerning definitions because B_x jumps only through a material contact discontinuity, where u and $u_\perp$ do not jump.

5.2 Relaxation system associated with Powell's system

In order to approximate (5.4) by relaxation, we just add the nonconservative part $\mathbf{u}\,\mathrm{div}\,\mathbf{B}$ of the Powell system to the magnetic equations of the relaxation system (2.1)–(2.8), and obtain

$$\begin{aligned}
&\rho_t + (\rho u)_x = 0,\\
&(\rho u)_t + (\rho u^2 + \pi)_x = 0,\\
&(\rho u_\perp)_t + (\rho u u_\perp + \pi_\perp)_x = 0,\\
&E_t + [(E + \pi)u + \pi_\perp \cdot u_\perp]_x = 0,\\
&(B_x)_t + u(B_x)_x = 0,\\
&(B_\perp)_t + (B_\perp u - B_x u_\perp)_x + u_\perp (B_x)_x = 0,
\end{aligned} \tag{5.5}$$

with still (1.6), and no change in the other equations

$$\begin{aligned}
&(\rho\pi)_t + (\rho\pi u)_x + (|b|^2 + c_b^2)u_x - c_a b \cdot (u_\perp)_x = 0,\\
&(\rho\pi_\perp)_t + (\rho\pi_\perp u)_x - c_a b\, u_x + c_a^2 (u_\perp)_x = 0,
\end{aligned} \tag{5.6}$$

$$(c_a)_t + u(c_a)_x = 0, \quad (c_b)_t + u(c_b)_x = 0, \quad b_t + u b_x = 0. \tag{5.7}$$

The studies made previously in [5] and in the present paper for the case $B_x = cst$ are valid in the more general case B_x non constant, the only difference being that now B_x has to be understood as evaluated locally (as it was the case for c_a, c_b, b).

5.3 Numerical fluxes

Computing the solution to the Riemann problem associated to the relaxation system gives an approximate Riemann solver for the Powell system. Then, one wants to compute the numerical fluxes associated to it. For the conservative quantities ρ, ρu, $\rho u_\perp$, E, they are given by the corresponding components of (2.14), with the additional information that B_x only jumps at the middle wave. For updating the magnetic quantities B_x and $B_\perp$, one has to be more careful since we are solving nonconservative equations. In the spirit of approximate Riemann solvers, one has to write that the new value $\mathbf{B}_i^{n+1}$ is obtained as the average over the cell of the approximate solution. The approximate solution satisfies

$$\mathbf{B}_t + (\mathbf{B}u - B_x\mathbf{u})_x + \mathbf{u}(B_x)_x = 0, \tag{5.8}$$

where $\mathbf{u} = (u, u_\perp)$. Denote by u^* the value of u through the material contact. Then one has

$$B_x = \begin{cases} B_x^l & \text{if } \dfrac{x}{t} < u^*, \\ B_x^r & \text{if } \dfrac{x}{t} > u^*. \end{cases} \tag{5.9}$$

But since

$$(B_x)_x = (B_x^r - B_x^l)\delta(x - tu^*), \qquad \mathbf{u}(B_x)_x = \mathbf{u}^*(B_x^r - B_x^l)\delta(x - tu^*), \tag{5.10}$$

where $\mathbf{u}^*$ is the value of $\mathbf{u}$ through the material contact, one has

$$[\mathbf{B}u - B_x\mathbf{u}]_{x=0} + \mathbf{u}^*(B_x^r - B_x^l)\mathbf{I}_{u^*=0} = 0, \tag{5.11}$$

where $[\ldots]_{x=0}$ denotes the jump through the line $x = 0$.

Now, integrate (5.8) over $(0, \Delta t) \times (-\Delta x, 0)$. We get

$$\frac{1}{\Delta x}\int_{-\Delta x}^{0} \mathbf{B}(x/\Delta t)dx - \mathbf{B}_l + \frac{\Delta t}{\Delta x}\left((\mathbf{B}u - B_x\mathbf{u})_{0-} - (\mathbf{B}u - B_x\mathbf{u})_l\right) + \frac{\Delta t}{\Delta x}\mathbf{u}^*(B_x^r - B_x^l)\mathbf{I}_{u^*<0} = 0. \tag{5.12}$$

Next, integrate (5.8) over $(0, \Delta t) \times (0, \Delta x)$. We get

$$\frac{1}{\Delta x}\int_0^{\Delta x} \mathbf{B}(x/\Delta t)dx - \mathbf{B}_r + \frac{\Delta t}{\Delta x}\left((\mathbf{B}u - B_x\mathbf{u})_r - (\mathbf{B}u - B_x\mathbf{u})_{0+}\right) + \frac{\Delta t}{\Delta x}\mathbf{u}^*(B_x^r - B_x^l)\mathbf{I}_{u^*>0} = 0. \tag{5.13}$$

Denote

$$\begin{aligned} F_l^{\mathbf{B}} &= (\mathbf{B}u - B_x\mathbf{u})_{0-} + \mathbf{u}^*(B_x^r - B_x^l)\mathbf{I}_{u^*<0}, \\ F_r^{\mathbf{B}} &= (\mathbf{B}u - B_x\mathbf{u})_{0+} - \mathbf{u}^*(B_x^r - B_x^l)\mathbf{I}_{u^*>0}. \end{aligned} \tag{5.14}$$

We end up with

$$\mathbf{B}_i^{n+1} - \mathbf{B}_i^n + \frac{\Delta t}{\Delta x}\left((F_l^{\mathbf{B}})_{i+1/2} - (F_r^{\mathbf{B}})_{i-1/2}\right) = 0. \tag{5.15}$$

According to (5.11), a formula for the numerical fluxes is

$$\text{If } u^* \geq 0 \text{ then } \begin{cases} F_l^{\mathbf{B}} = (\mathbf{B}u - B_x\mathbf{u})_{0-}, \\ F_r^{\mathbf{B}} = (\mathbf{B}u - B_x\mathbf{u})_{0-} - \mathbf{u}^*(B_x^r - B_x^l), \end{cases} \tag{5.16}$$

$$\text{If } u^* \leq 0 \text{ then } \begin{cases} F_l^{\mathbf{B}} = (\mathbf{B}u - B_x\mathbf{u})_{0+} + \mathbf{u}^*(B_x^r - B_x^l), \\ F_r^{\mathbf{B}} = (\mathbf{B}u - B_x\mathbf{u})_{0+}. \end{cases} \tag{5.17}$$

In all cases one has

$$F_r^{\mathbf{B}} - F_l^{\mathbf{B}} = -\mathbf{u}^*(B_x^r - B_x^l), \tag{5.18}$$

which implies a consistent discretization of the nonconservative term in (5.8). Notice that the above derivation of the left and right numerical fluxes $F_l^{\mathbf{B}}$, $F_r^{\mathbf{B}}$ involved in (5.15) does not really use the relaxation system, but merely only (5.8), which is indeed the exact induction equation of Powell's system. Thus the formulas are true also for the exact Riemann solver, for example.

This relaxation solver is positive and entropy satisfying under the same conditions that are derived in [5]. The only modification is that B_x has always to be understood as evaluated locally, according to (5.9). For the 3- and 5-wave solvers, Propositions 3.2 and 3.3 remain valid with this interpretation, as well as the formulas for the intermediate states.

References

1. Barth, T.J.: Numerical methods for gasdynamic systems on unstructured meshes. In: Dietmar, K., Mario, O., Christian, R. (eds.) An Introduction to Recent Developments in Theory and Numerics for Conservation Laws: Proceedings of the International School on Theory and Numerics and Conservation Laws, Freiburg/Littenweiler, October 20–24, 1997, pp. 195–285. Springer, Berlin (1999)

2. Bouchut, F.: Entropy satisfying flux vector splittings and kinetic BGK models. Numer. Math. **94**(4), 623–672 (2003)
3. Bouchut, F.: Nonlinear stability of finite volume methods for hyperbolic conservation laws and well-balanced schemes for sources. Frontiers in Mathematics, vol. 8, 135 p, Birkhäuser, Basel (2004)
4. Bouchut, F., Klingenberg, C., Waagan, K.: A multiwave approximate riemann solver for ideal mhd based on relaxation III—numerical implementation with 7 waves. (To appear)
5. Bouchut, F., Klingenberg, C., Waagan, K.: A multiwave approximate riemann solver for ideal mhd based on relaxation I—theoretical framework. Numer. Math. **108**(1), 7–41 (2007)
6. Brio, M., Wu, C.C.: An upwind differencing scheme for the equations of ideal magnetohydrodynamics. J. Comput. Phys. **75**(2), 400–422 (1988)
7. Dai, W., Woodward, P.R.: An approximate Riemann solver for ideal magnetohydrodynamics. J. Comput. Phys. **111**(2), 354–372 (1994)
8. Falle, S.A.E.G., Komissarov, S.S., Joarder, P.: A multidimensional upwind scheme for magnetohydrodynamics. Mon. Notices R. Astron. Soc. **297**(1), 265–277 (1998)
9. Gurski, K.F.: An HLLC-type approximate Riemann solver for ideal magnetohydrodynamics. SIAM J. Sci. Comput. **25**(6), 2165–2187 (2004)
10. Li, S.: An HLLC Riemann solver for magneto-hydrodynamics. J. Comput. Phys. **203**(1), 344–357 (2005)
11. Miyoshi, T., Kusano, K.: A multi-state HLL approximate Riemann solver for ideal magnetohydrodynamics. J. Comput. Phys. **208**(1), 315–344 (2005)
12. Powell, K.G.: An approximate Riemann solver for magnetohydrodynamics (that works in more than one dimension). Technical report, Institute for Computer Applications in Science and Engineering (ICASE) (1994)